JOURNAL OF GEOPHYSICAL RESEARCH, VOL. 105, NO. A5, 10519–10526, DOI:10.1029/1999JA000297, 2000

New kinetic instability: Oblique Alfvén fire hose

P. Hellinger and H. Matsumoto

Radio Atmospheric Science Center, Kyoto University, Uji, Japan

Abstract. Two instabilities could take place in plasma with a bi-Maxwellian proton distribution function with $T_{p\|} > T_{p\perp}$, where $T_{p\|}$ and $T_{p\perp}$ are proton temperatures, parallel and perpendicular, respectively, to the background magnetic field. The first instability is the fire hose (or whistler fire hose), generating low-frequency whistler waves at parallel propagation. We found a new, second instability, the Alfvén fire hose, that generates zero-frequency waves of the Alfvén branch at strongly oblique propagation. The Alfvén fire hose has a linear growth rate comparable to or even greater than that of the whistler fire hose. The two instabilities with the same initial plasma parameters are examined via one-dimensional hybrid simulations and turn out to have behavior very different from each other. The whistler fire hose has an overall quasi-linear evolution, while the evolution of the Alfvén fire hose is more complicated: Initially, unstable zero-frequency waves are gradually transformed into propagating Alfvén waves; during this process the waves are strongly damped and heat protons in a perpendicular direction. Consequently, the Alfvén fire hose is very efficient at destroying proton anisotropy.

1. Introduction

Many processes in a collisionless plasma lead to the development of particle temperature anisotropy. The anisotropic plasma generates instabilities which are often kinetic by their very nature. The instabilities reduce the anisotropy and affect the global plasma properties; the generated waves and anisotropy determine, for example, characteristic macrophysical speeds [*Karimabadi et al.*, 1995] and polytropic indices [*Belmont and Mazelle*, 1992].

An instability typically ends in a state of marginal stability [*Manheimer and Boris*, 1977, and references therein] where generated waves are almost undamped. When the instability has an overall quasi-linear evolution (so there are no important nonlinear effects such as particle trapping and wave-wave coupling), the marginal stability state is identical to the instability threshold, given by linear theory. Many authors used the above arguments to determine constraints on temperature anisotropy from linear theory and numerical simulations [*Gary et al.*, 1998, and references therein].

Recently, *Gary et al.* [1998] studied the properties of a plasma with the anisotropic proton distribution function with $T_{p\|} > T_{p\perp}$, where $T_{p\|}$ and $T_{p\perp}$ are proton temperatures parallel and perpendicular, respectively, to the background magnetic field. *Gary et al.* [1998; see also *Quest and Shapiro*, 1996] have shown that the anisotropic protons destabilize the low-frequency (below proton cyclotron frequency) whistler branch via fire hose instability; hereinafter we call this instability the whistler fire hose for reasons which become clear below. *Gary et al.* [1998] have studied in detail the linear properties of the whistler fire hose and have shown, using hybrid simulations, that the instability has an overall quasi-linear behavior. On the basis of arguments of marginal stability analysis [*Manheimer and Boris*, 1977], and on linear analysis as well as on the simulation results, *Gary et al.* [1998] gave a prediction of the constraints of proton anisotropy.

In this paper we show that a plasma with $T_{p\perp} < T_{p\|}$ may drive another, new instability that destabilizes a zero-frequency part of the Alfvén branch; we find, surprisingly, that Alfvén waves have complex dispersive properties in higher beta plasmas, including anomalous dispersion and zero-frequency modes. The zero-frequency waves are generally strongly damped, but in plasma with anisotropic protons $T_{p\perp} < T_{p\|}$ these waves become unstable. The new instability has many properties similar to those of the classical MHD-CGL fire hose; for this reason we call this instability the "Alfvén fire hose." We study the linear properties and find that the Alfvén fire hose is competitive with, and even dominates, the whistler fire hose at the linear stage. We also perform one-dimensional (1-D) hybrid simulations of the two instabilities. Whereas the whistler fire hose exhibits a quasi-linear behavior, the nonlinear evolution of the Alfvén fire hose is much more complicated and its final plasma state is far from the instability threshold.

This paper is organized as follows: In section 2 we describe results of linear theory for the Alfvén fire hose (section 2.2) and its relation to Alfvén waves (section 2.1). In section 3 we examine results of 1-D hybrid simulations for the whistler and Alfvén fire hoses. Finally, in section 4 we discuss the results and their implications.

2. Linear Theory

In this section we show results of our dispersion solver [*Hellinger and Mangeney*, 1999] for a homogeneous plasma with bi-Maxwellian protons and electrons. We assume there is no relative drift between electrons and protons and that the charge neutrality holds. The units and parameters of the dispersion solver are the following: Units of wave vector $\boldsymbol{k}$ (and its amplitude k) and frequency ω are ω_{pi}/c and Ω_i, respectively, where $\omega_{pi} = (n_p e^2/m_p \epsilon_0)^{1/2}$ is the proton plasma frequency and $\Omega_i = eB_0/m_p$ is the proton gyrofrequency. In these expressions, n_p and B_0 are the density of the plasma protons and magnitude of the background magnetic field $\boldsymbol{B}_0$, respectively, while e and m_p are the proton electric charge and mass, respectively; finally, c and ϵ_0 are the speed of light and the permittivity of vacuum, respectively. These same units are used in all our figures. The relevant plasma parameters are the ratio $T_{p\perp}/T_{p\|}$, and plasma betas, ratios between particle pressures and the magnetic pressure $p_B = B_0^2/(2\mu_0)$: the electron beta $\beta_e = n_p k_B T_e/p_B$, and the proton parallel beta $\beta_{p\|} = n_p k_B T_{p\|}/p_B$, where k_B is Boltzmann constant, μ_0 is permeability of vacuum, and T_e is electron temperature. For isotropic protons ($T_{p\perp} = T_{p\|} = T_p$) we use the proton beta $\beta_p = n_p k_B T_p/p_B$.

The anisotropic proton distribution function with $T_{p\perp} < T_{p\|}$ destabilizes the right-handed, low-frequency whistler mode via the whistler fire hose [*Gary et al.*, 1998]. The unstable waves are generally resonant, have nonzero real frequency, and have maximum growth rate at parallel propagation with respect to the background magnetic field. However, we find that anisotropic protons not only

0148-0227/05/1999JA000297$9.00

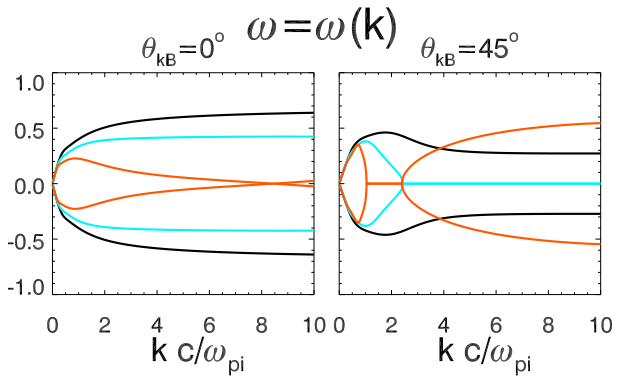

Plate 1. Linear theory: Alfvén wave dispersion $\omega = \omega(k)$ for (left) $\theta_{\boldsymbol{kB}} = 0^{\circ}$ and (right) $\theta_{\boldsymbol{kB}} = 45^{\circ}$ for isotropic plasmas with β_e and β_p equal to 1/2 (black curve), 1 (blue curve), and 2 (red curve).

destabilize the resonant whistler fire hose but also lead to a new instability: The Alfvén fire hose. Since the Alfvén fire hose is intimately connected with the Alfvén wave dispersion in hot plasmas, we study in detail the properties of Alfvén waves in the next section.

2.1. Alfvén Waves

In homogeneous, Maxwellian plasmas, Alfvén waves are nondispersive, $\omega \propto k$, and almost nondamped for long wavelengths $k \ll \omega_{pi}/c$. For shorter wavelengths the proton cyclotron resonance $\omega - kv = \Omega_i$ damps Alfvén waves and leads to a dispersive behavior:

$$\partial^2\omega(k,\theta_{\boldsymbol{kB}})/\partial k^2 < 0, \tag{1}$$

where $\theta_{\boldsymbol{kB}}$ is the angle between the $\boldsymbol{k}$ vector and the background magnetic field $\boldsymbol{B}_0$. In a cold plasma the frequency of Alfvén waves monotonically increases as k increases and approaches $\omega_\infty \sim \Omega_i \cos\theta_{\boldsymbol{kB}}$ as $k \to \infty$ for $\theta_{\boldsymbol{kB}} < 80^{\circ}$. However, the situation is more complicated in a hot plasma: For higher β the dispersion becomes anomalous with

$$\partial\omega(k,\theta_{\boldsymbol{kB}})/\partial k < 0. \tag{2}$$

For parallel propagation the frequency reaches zero and even changes sign. For oblique propagation the dispersion is even more "exotic": The two oppositely propagating Alfvén waves reach zero frequency and convert themselves to two zero-frequency modes; for shorter wavelengths, Alfvén waves reappear with a changed frequency sign (and therefore right-handed polarization). To certify the above statements, we show results from the dispersion solver in Plate 1. Plate 1 shows three examples of Alfvén waves dispersion, $\omega = \omega(k)$ for parallel, $\theta_{\boldsymbol{kB}} = 0^{\circ}$, propagation (left panel), and oblique, $\theta_{\boldsymbol{kB}} = 45^{\circ}$, propagation (right panel), for isotropic plasmas with β_e and β_p equal to $1/2$ (black curve), 1 (blue curve), and 2 (red curve). Note that we assume k positive and show modes with positive and negative frequencies ω. Plate 1 (left panel, red curve) shows the actual crossing of two oppositely propagating Alfvén waves at $\omega = 0$ at about $k = 8$ for $\beta_p = \beta_e = 2$. Plate 1 (right panel) shows the zero-frequency modes for $\beta_e = \beta_p = 1$ (blue curve) for $k > 2$ and for $\beta_e = \beta_p = 2$ (red curve) for k between 1 and 2.

Plate 1 also shows that a 2-D view of the dispersion relation $\omega = \omega(k, \theta_{\boldsymbol{kB}})$ is necessary to have a full picture of the properties of Alfvén waves. Before we proceed further we note that the waves of short wavelength (including the zero-frequency modes) are strongly damped in the isotropic plasmas. For this reason, let us concentrate on the properties of anisotropic plasmas.

As the ratio $T_{p\perp}/T_{p\parallel}$ decreases and/or β_p ($\beta_{p\parallel}$) increases, the complicated behavior of Alfvén waves becomes more pronounced: The zero-frequency region approaches longer wavelengths. A typical example of the dispersion properties is shown in Plate 2.

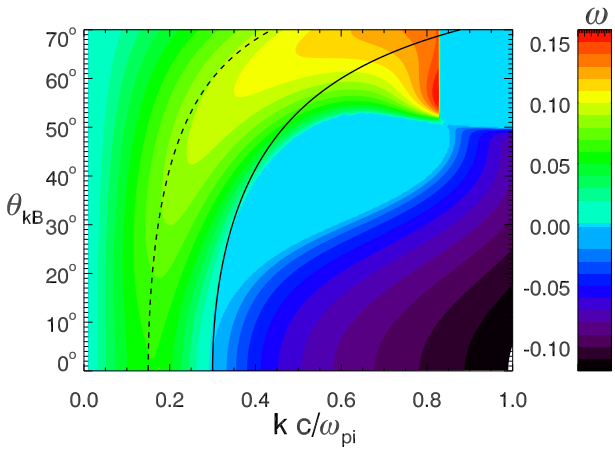

Plate 2. Linear theory, $\beta_{p\parallel} = 2.8$, $T_{p\perp}/T_{p\parallel} = 0.6$: Alfvén wave dispersion ω as a function of k and $\theta_{\boldsymbol{kB}}$ shown as a two-dimensional (2-D) color scale plot (the color scale used is displayed at right). Solid and dashed curves denote $k_\parallel = k\cos\theta_{\boldsymbol{kB}}$ that equals 0.3 and 0.15, respectively.

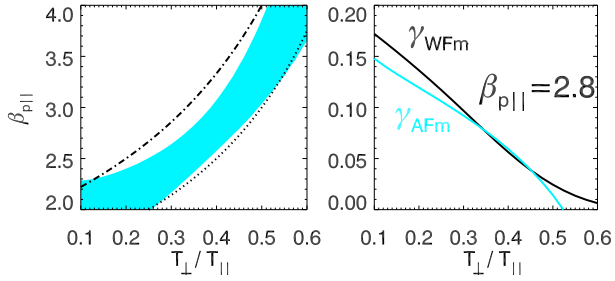

Plate 3. Linear theory: (left) Blue area shows a region in $(T_{p\perp}/T_{p\parallel}, \beta_{p\parallel})$ space where the maximum growth rate of the Alfvén fire hose γ_{AFm} is greater than the maximum growth rate of the whistler fire hose γ_{WFm}. Overlain curves denote the relations $\beta_{p\parallel}(1 - T_{p\perp}/T_{p\parallel})$ equal to 2 (dash-dotted curve) and 1.5 (dotted curve). (right) Maximum growth rates γ_{WFm} (black curve) and γ_{WFm} (blue curve) as a function of $T_{p\perp}/T_{p\parallel}$ for $\beta_{p\parallel} = 2.8$

Plate 2 shows a 2-D color scale plot of the dispersion relation of Alfvén waves, ω, as a function of k and $\theta_{\boldsymbol{kB}}$ for $\beta_{p\parallel} = 2.8$ and $T_{p\perp}/T_{p\parallel} = 0.6$ (hereinafter, we use the ad hoc value $\beta_e = 0.5$); the solid and dashed curves denote $k_\parallel = k\cos\theta_{\boldsymbol{kB}}$ that equals 0.3 and 0.15, respectively.

Plate 2 shows that the dispersion properties of Alfvén waves are indeed complicated. There are three qualitatively different dispersion relations $\omega = \omega(k)$ for a fixed $\theta_{\boldsymbol{kB}}$.

1. For $\theta_{\boldsymbol{kB}} < 50^{\circ}$, ω increases as k increases for long wavelengths, then crosses a turning point $\partial\omega/\partial k = 0$, and eventually changes sign. For $10^{\circ} < \theta_{\boldsymbol{kB}} < 50^{\circ}$ and $0.3 < k < 0.8$, the Alfvén branch contains a wide region of zero-frequency waves (light blue region).

2. For $50^{\circ} < \theta_{\boldsymbol{kB}} < 52^{\circ}$, ω increases as k increases for long wavelengths, then crosses a turning point, and reaches zero. After the zero-frequency region, ω increases and decreases again, and eventually reaches zero, giving rise to the second zero-frequency region.

3. For $\theta_{\boldsymbol{kB}} > 52^{\circ}$, ω is always positive, increases as k increases for long wavelengths, then crosses a turning point $\partial\omega/\partial k = 0$, and then decreases to another turning point $\partial\omega/\partial k = 0$, and eventually increases as k increases. The abrupt change of frequency for $k \sim 0.83$ is due to a jump between two branches, as the dispersion solver tried to continue on the first branch but failed and moved to the second branch of dispersion relation (for $50^{\circ} < \theta_{\boldsymbol{kB}} < 52^{\circ}$).

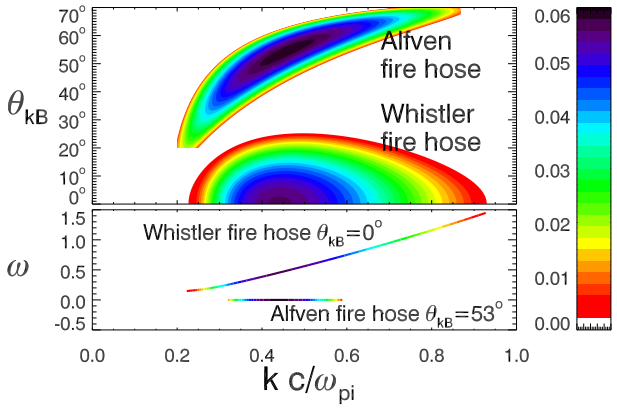

Plate 4. Linear theory, $\beta_{p\|} = 2.8$, $T_{p\perp}/T_{p\|} = 0.4$: (top) Growth rate $\gamma = \gamma(k, \theta_{\boldsymbol{kB}})$ of the Alfvén and whistler fire hoses shown as a 2-D color scale plot. (the color scale used is displayed at right). (bottom) Frequency $\omega = \omega(k)$ of unstable waves for the whistler fire hose at $\theta_{\boldsymbol{kB}} = 0^{\circ}$ and the Alfvén fire hose at $\theta_{\boldsymbol{kB}} = 53^{\circ}$. The curves $\omega = \omega(k)$ are colored using the growth-rate color scale displayed at right.

The second zero-frequency region and generally short-wavelength waves are of low interest since they are strongly damped.

A closer look at Plate 2 reveals that the turning points $\partial\omega/\partial k = 0$ are near the curve satisfying the relation $k_{\|} = 0.15$. Similarly, the zero-frequency region (light blue) is also mainly governed by a relation $k_{\|} \sim$ const (see Plate 2, solid curve); this feature suggests that the cyclotron resonance,

$$k_{\|} = \frac{\omega \pm \Omega_i}{v_{\rm res}} \tag{3}$$

($v_{\rm res}$ denotes resonant velocity), plays an important role. Indeed, for $\omega \ll \Omega_i$ and $v_{\rm res} \sim$ const we have $k_{\|} = \pm\Omega_i/v_{\rm res} \sim$ const. On the other hand, the zero-frequency waves, with $k_{\|} \sim 0.3 - 0.5$, are not strongly (cyclotron) resonant with the protons, since the resonant protons with the velocity $|v_{\rm res}| \sim 2 - 3v_A$ fall to the tail region of the distribution function.

So far the Alfvén branch (including the zero-frequency modes) was stable. This is no longer true if the anisotropy gets stronger, as we shall see in the next section.

2.2. Alfvén Fire Hose

If the anisotropy exceeds a threshold, which we find near the relation

$$\beta_{p\|}(1 - T_{p\perp}/T_{p\|}) \sim 1.4 \tag{4}$$

for $2 < \beta_{p\|} < 4$, one of the zero-frequency modes becomes unstable, with a maximum growth rate at oblique propagation with respect to the background magnetic field. The unstable zero-frequency mode shares many properties with the MHD-CGL fire hose: It is linearly polarized,

$$\delta\boldsymbol{B} = \delta B \boldsymbol{n} \tag{5}$$

(where $\boldsymbol{n}$ is a unit vector parallel to $\boldsymbol{k} \times \boldsymbol{B}_0$), is nonresonant, and is purely growing, $\omega = 0$. Therefore we call the instability (and the mode) the Alfvén fire hose. The main difference between the Alfvén fire hose and the MHD-CGL fire hose is that the latter has maximum growth rate at parallel propagation. This is because the MHD-CGL neglects the cyclotron kinetic effects, which are in this case important.

The obliquely propagating Alfvén fire hose is compressible $\delta n \neq 0$ with the compressibility ratio

$$(\delta n/n)/(|\delta\boldsymbol{B}|/B_0) \sim 0.1.$$

Fluctuating quantities δn and δB (equation (5)) are correlated

$$\delta n = \alpha \delta B, \tag{6}$$

where the coefficient α is negative if $\boldsymbol{n} \cdot \boldsymbol{k} \times \boldsymbol{B}_0$ is positive (and vice versa).

The features of the Alfvén fire hose as the linear polarization and the anticorrelation between δn and δB (equation (6)) are important for the recognition of the Alfvén fire hose. However, these properties are predicted by linear theory, and whether they are plausible even for the nonlinear stage of the instability evolution is a problem we investigate in section 3.

Let us now compare the growth rates of the Alfvén and whistler fire hoses for bi-Maxwellian plasma. Results of an exploration for plasmas with $0.1 < T_{p\perp}/T_{p\|} < 0.6$ and $2 < \beta_{p\|} < 4$ are shown in Plate 3. Plate 3 (left panel) shows a blue area, a region in $(T_{p\perp}/T_{p\|}, \beta_{p\|})$ space where the maximum growth rate of the Alfvén fire hose γ_{AFm} is greater than the maximum growth rate of the whistler fire hose γ_{WFm}. The dash-dotted curve denotes the relation $\beta_{p\|}(1 - T_{p\perp}/T_{p\|}) = 2$ (the threshold of the MHD-CGL fire hose), while the dotted curve denotes $\beta_{p\|}(1 - T_{p\perp}/T_{p\|}) = 1.5$. Plate 3 (right panel) displays growth rates γ_{WFm} and γ_{AFm} (blue curve) as a function of $T_{p\perp}/T_{p\|}$ for $\beta_{p\|} = 2.8$. From Plate 3 we conclude that in moderately hot plasmas with $2 < \beta_{p\|} < 4$, the Alfvén fire hose dominates over the whistler fire hose for approximately

$$1.5 < \beta_{p\|}(1 - T_{p\perp}/T_{p\|}) < 1.9. \tag{7}$$

It is interesting to note that for some plasma parameters (see Plate 3, right panel) the Alfvén fire hose is stabilized while the whistler fire hose is unstable [cf. *Gary et al.*, 1998].

Another comparison between growth rates of the instabilities for one case is shown in Plate 4. Plate 4 (top panel) displays the growth rate as a function of k and $\theta_{\boldsymbol{kB}}$ shown as a 2-D color scale plot (the color scale used is displayed at right) for the Alfvén fire hose and the whistler fire hose for $\beta_{p\|} = 2.8$, and $T_{p\perp}/T_{p\|} = 0.4$ (the case we study in section 3 using a hybrid code). Note that the two islands of instability in Plate 4 (top panel) correspond to two different branches with quite different frequency regimes: Plate 4 (bottom panel) shows the frequency $\omega = \omega(k)$ of unstable waves for the whistler fire hose at $\theta_{\boldsymbol{kB}} = 0^{\circ}$ and the Alfvén fire hose at $\theta_{\boldsymbol{kB}} = 53^{\circ}$. The curves $\omega = \omega(k)$ are colored using the growth-rate color scale displayed at right. Both the instabilities are unstable for a wide region of $\boldsymbol{k}$ vectors and have comparable maximum growth rate. The Alfvén fire hose has a slightly greater maximum growth rate ($\gamma_{\rm AFm} = 0.059$) than the whistler fire hose ($\gamma_{\rm WFm} = 0.056$) in this case (see Plate 3).

The growth rates of the two instabilities are also influenced by electrons. Electrons are nonresonant for the two instabilities but may significantly change the plasma dispersion properties and therefore the growth rate. For isotropic electrons, when increasing the temperature the growth rate of the whistler fire hose is nearly constant but that of the Alfvén fire hose slowly increases. As for the electron temperature anisotropy, when the ratio $T_{e\perp}/T_{e\|}$ increases, the maximum growth rate decreases (and vice versa) for the whistler fire hose [*Kennel and Scarf*, 1968; *Hollweg and Völk*, 1970], as well as for the Alfvén fire hose, and we have found that the growth rate for the two instabilities decreases at comparable speeds.

Linear theory suggests that the Alfvén fire hose is important in the context of space plasma physics, since it is competitive with, and even dominates, the whistler fire hose. The two instabilities and their linear competition are only slightly influenced by electrons, and therefore a hybrid code which treats electrons as a massless fluid is a suitable tool for a study of their nonlinear behavior [*Gary et al.*, 1998]. In the next section we perform 1-D hybrid simulations of the two instabilities and compare their results.

3. Simulations

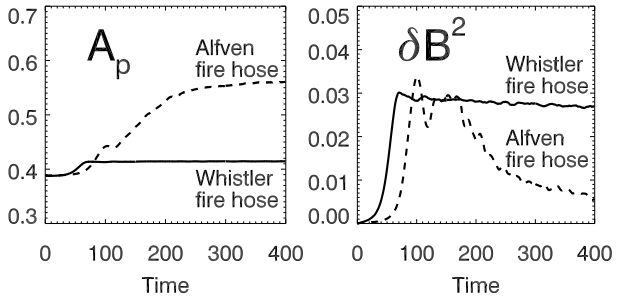

Figure 1. Simulation results for initial conditions $\beta_{p\|} = 2.8$ and $T_{p\perp}/T_{p\|} = 0.4$: Evolution of (left) temperature anisotropy $A_p = T_{p\perp}/T_{p\|}$ and (right) magnetic fluctuation δB^2 for the whistler fire hose (solid curve) at $\theta_{\boldsymbol{kB}} = 0^\circ$ and the Alfvén fire hose (dashed curve) at $\theta_{\boldsymbol{kB}} = 53^\circ$.

For the numerical simulations we use the 1-D version of the hybrid code developed by *Matthews* [1994]. In this code the electrons are considered as a massless fluid, with a constant temperature; the ions are treated as particles and advanced by a leapfrog scheme which requires the fields to be known at half time steps ahead of the particle velocities; this is obtained by advancing the current density to this time step with only one computational pass through the particle data at each time step. Two interlaced grids are used, one with nodes at cell centers for the electric field and the other one with nodes at cell vertices for all the other fields. The particle contribution to the current density at the relevant nodes is evaluated with bilinear weighting. No smoothing is performed on the electromagnetic fields, and the resistivity is set to zero in Ohm's law. The magnetic field is advanced in time with a modified midpoint method, which allows time substepping for the advance of the field.

The units and parameters of the simulation are identical to those of the dispersion solver (section 2): Units of space and time are c/ω_{pi} and $1/\Omega_i$, respectively. The spatial resolution is $dx = c/\omega_{pi}$. There are $10,240$ particles per cell. The simulation box is along the x axis and is assumed to be periodic. The fields and moments are defined on a 1-D grid of 1024 points. The time step for the particle advance is $dt = 0.02\Omega_i^{-1}$, while the magnetic field **B** is advanced with a smaller time step, $dt_B = dt/10$. Velocities are given in units of v_A, and the magnetic field is in units of B_0, where v_A is the Alfvén velocity. The same units are used in all subsequent figures.

We initialize the simulation with homogeneous, anisotropic protons, $\beta_{p\|} = 2.8$, and $T_{p\perp}/T_{p\|} = 0.4$. Electrons are isotropic and have $\beta_e = 0.5$. We perform two simulations: The first one for the study of the whistler fire hose, where the initial homogeneous magnetic field is along the x axis, $\boldsymbol{B}_0 = (1, 0, 0)$, and the second one for the study of the Alfvén fire hose, where the initial magnetic field is $\boldsymbol{B}_0 = (\cos\theta_{\boldsymbol{kB}}, \sin\theta_{\boldsymbol{kB}}, 0)$, where $\theta_{\boldsymbol{kB}} = 53^\circ$. Let us now look at the simulation results.

3.1. Nonlinear Evolution

Quest and Shapiro [1996] and *Gary et al.* [1998] have shown that the whistler fire hose evolves and saturates in a quasi-linear manner. In agreement with *Quest and Shapiro* [1996] and *Gary et al.* [1998], we observe a similar evolution. So hereinafter we concentrate on the Alfvén fire hose and on the comparison of its evolution with that of the whistler fire hose.

As the linear properties of the Alfvén and whistler fire hoses differ, so do their nonlinear evolutions. Indeed, in Figure 1 we compare the evolution of the Alfvén fire hose with that of the whistler fire hose in the two hybrid simulations. Figure 1 shows the evolution of temperature anisotropy $A_p = T_{p\perp}/T_{p\|}$ (left panel) and magnetic fluctuation δB^2 (right panel) during the simulations for the whistler fire hose (solid curve) and the Alfvén fire hose (dashed curve). During the linear stage, both instabilities grow for large number of $\boldsymbol{k}$ vectors with the predicted linear growth rates. Fluctuating magnetic field energy density δB^2 grows faster for the whistler fire hose than for the Alfvén fire hose because the $\boldsymbol{k}$ region of unstable waves is wider for the whistler fire hose (see Plate 4, bottom panel); moreover, the initial noise dominates at parallel propagation.

Figure 1 illustrates the fact that the whistler fire hose has a quasi-linear evolution (right panel): Magnetic fluctuation saturates at a certain level and stays at about this level after the saturation. The anisotropy slightly decreases to a level where the destabilized waves are marginally stable.

The Alfvén fire hose presents a different evolution (Figure 1, dashed curve): The waves grow, saturate, and then are rather strongly damped for time >180. The damping results in an important reduction of anisotropy as Figure 1 (left panel) evidences.

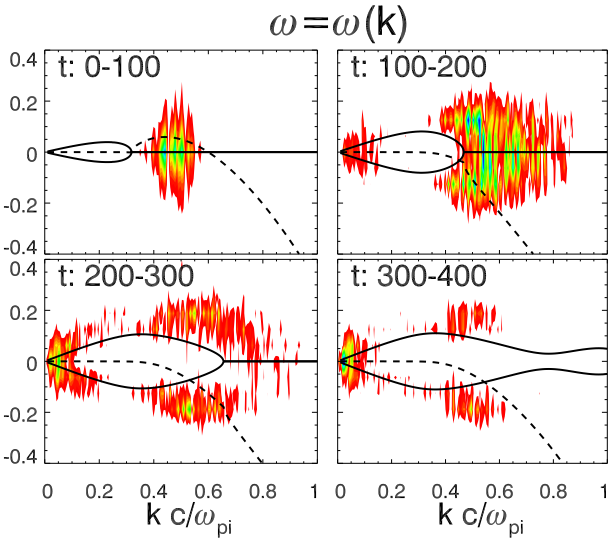

Plate 5. Simulation results for the Alfvén fire hose at $\theta_{\boldsymbol{kB}} = 53^\circ$: Spectrum $\omega = \omega(k)$, as a color scale plot, at different time intervals. The same scale was used for all four panels. Curves denote prediction of linear theory, using corresponding, time-averaged proton temperatures, and assuming that the protons have bi-Maxwellian distribution (solid curve is $\omega = \omega(k)$ and dashed curve is $\gamma = \gamma(k)$).

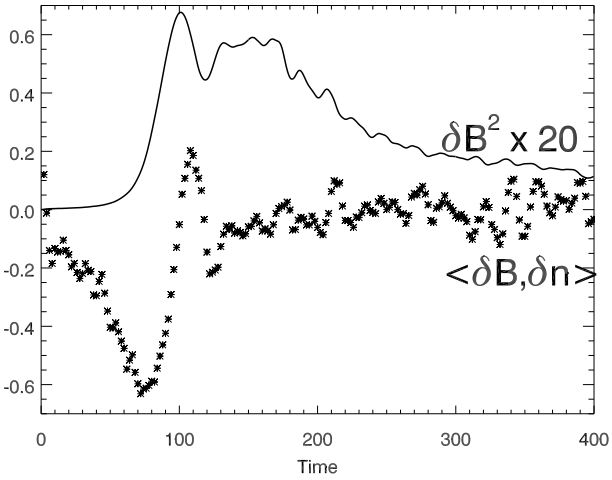

Figure 2. Simulation results for the Alfvén fire hose at $\theta_{\boldsymbol{kB}} = 53^\circ$: Evolution of the magnetic fluctuation δB^2 (solid curve) and the correlation between δB and δn, $\langle \delta B, \delta n \rangle$ (asterisks).

The Alfvén fire hose is (in the present case) more efficient at reducing the anisotropy than the whistler fire hose. Let us now study the evolution of the Alfvén fire hose in detail so as to determine why its evolution is so different from that of the whistler fire hose.

3.2. Alfvén Fire Hose and Alfvén Waves

Let us first recall that the Alfvén fire hose is a result of the complicated dispersion of Alfvén waves (see section 2.1); in a region where we usually see Alfvén waves in isotropic plasma, there exists an unstable, zero-frequency mode in a plasma with anisotropic protons. This feature is the key to understanding the nonlinear evolution of the Alfvén fire hose.

Initially, the Alfvén fire hose grows for a wide range of $\boldsymbol{k}$ vectors with linearly polarized magnetic fluctuations $\delta B = B_z$; $B_x, B_y \sim$ const. As the amplitude of the waves becomes important, quasi-linear effects appear, and the waves start to heat protons mainly in the perpendicular direction. At this moment the dispersion properties turn out to be important. As the temperature anisotropy reduces, the dispersion changes: The zero-frequency region displaces. As consequence, an initially unstable, zero-frequency mode with a given $\boldsymbol{k}$ vector sees the gradual change of dispersion property and eventually converts to "standard" Alfvén waves. Because the Alfvén fire hose is linearly polarized, the Alfvén waves inherit the linear polarization. The energy of the Alfvén fire hose is converted to a superposition of Alfvén waves propagating parallel and antiparallel with respect to the $\boldsymbol{k}$ vector. The conversion is a source of damping, and the resulting Alfvén waves are also damped (these two mechanisms are tightly connected, and one can hardly say which one is more important). The damping results in an additional proton heating (mainly in the perpendicular direction) and gives a positive feedback to the whole process. Finally, the anisotropy is strongly reduced and the wave activity is strongly damped.

Let us illustrate the above described process using the simulation data. Plate 5 shows the integrated spectra $\omega = \omega(k)$, as a color scale plot, in different time intervals (the same scale was used for all four panels); for the overall evolution see Figure 1. To compare the simulation results with the linear theory, we have overlain $\omega = \omega(k)$ (solid curve), and $\gamma = \gamma(k)$ (dashed curve), calculated using the dispersion solver for the time-averaged proton temperatures, and assuming the protons have bi-Maxwellian distribution.

Plate 5 (top left) shows the spectrum during the time 0–100, i.e., during the initial, mainly linear stage: Alfvén fire hose waves are generated at zero-frequency (with a finite frequency spread owing to the finite growth rate) in the region ($k \sim$0.3–0.6), where linear theory predicts instability. Plate 5 (top right) shows the spectrum during the time 100–200, i.e., during the period of saturation: Alfvén waves (with $k < 0.5$) coexist with zero-frequency mode (with $k > 0.5$). The linear prediction does not fit very well to the spectrum observed in the simulation because, as we shall see later, the protons are far from being bi-Maxwellian, and, moreover, the plasma parameters are changing during the time intervals; the same arguments also apply for the other panels, but at least linear theory shows a qualitative agreement with the simulation.

The two bottom panels of Plate 5 show that Alfvén waves are damped at time 200-400. Plate 5 (bottom right) also reveals that long-wavelength Alfvén waves (with $k < 0.2$) appear at later times of the simulation; they are elliptically polarized with $\delta B_y >> \delta B_z$. A natural explanation of this phenomenon is that a wave-wave coupling takes place between two short-wavelength Alfvén waves and one long wavelength. The condition for this wave-wave interaction is favorable since later on (Plate 5, bottom) Alfvén waves driven by the Alfvén fire hose are almost dispersionless, $\omega \propto k$, for $k < 0.6$.

To test if there exists a three-wave interaction, we have calculated the (modified) bicoherency $C(k_1, k_2)$ [cf. *Rezeau et al.*, 1997] of B_z and B_y components of magnetic field as follows:

$$C(k_1,k_2) = \frac{\langle B_z(k_1)B_y(k_2)B_z(k_1+k_2)^*\rangle}{\langle |B_z(k_1)B_y(k_2)B_z(k_1+k_2)^*|\rangle}, \qquad (8)$$

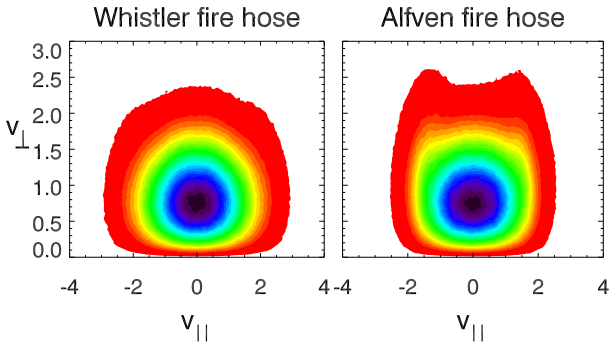

Plate 6. Simulation results: Proton distribution function $v_\perp f(v_\parallel, v_\perp)$, as color scale plot, of (left) the whistler fire hose at $\theta_{\boldsymbol{kB}} = 0^\circ$ and (right) the Alfvén fire hose at $\theta_{\boldsymbol{kB}} = 53^\circ$ at $t = 400$.

where $B_y(k)$ and $B_z(k)$ are

$$B_y(k,t) = \int B_y(x,t)\exp(ikx)dx$$
$$B_z(k,t) = \int B_z(x,t)\exp(ikx)dx$$

(in reality we perform discrete Fourier transform). Angle brackets denote the time average over the interval 200–400 (we use 101 samples of B_y and B_z), and the asterisks denote the complex conjugates. We have found significant bicoherency $C(k_1, k_2) \sim$0.75–0.99 among waves with $0.4 < k_1 < 0.8$, $k_2 < 0.15$, and $k_3 = k_1 + k_2$ (see Plate 5, bottom). This result suggests that the large-scale Alfvén waves are indeed generated by the wave-wave interaction, but further investigation of this phenomenon is beyond the scope of this paper.

Linear theory predicts that the Alfvén fire hose is compressible with the anticorrelation between δn and δB (see section 2.2). We have seen, however, that during the nonlinear evolution the Alfvén fire hose converts to Alfvén waves, so one may wonder what is happening with the phase between δn and δB. Figure 2 displays the evolution of magnetic fluctuation δB^2 (solid curve) and the correlation between δB and δn (asterisks), $\langle \delta B, \delta n\rangle$. Figure 2 shows that during the initial, linear stage the correlation $\langle \delta B, \delta n\rangle$ becomes significantly negative, which is in agreement with linear theory. Later on, however, the correlation swings to the positive value and oscillates with a low amplitude around zero. This effect is a consequence of the transformation of the Alfvén fire hose to Alfvén waves: Let us for simplicity suppose that the Alfvén fire hose of given $\boldsymbol{k}$ vector, $\boldsymbol{k} = (k, 0, 0)$, in a frame where $\boldsymbol{B}_0 = (\cos 53^\circ, \sin 53^\circ, 0)$, generates two linearly polarized Alfvén waves of the same amplitude, propagating parallel and antiparallel with respect to the $\boldsymbol{k}$ vector. The magnetic and density fluctuations then read as follows:

$$\begin{aligned} \delta B &\propto \cos(kx-\omega t) + \cos(kx+\omega t) \\ \delta n &\propto \cos(kx-\omega t-\phi) + \cos(kx+\omega t+\phi), \end{aligned} \qquad (9)$$

where ω is the wave frequency and ϕ is the phase difference between δn and δB. The angle ϕ is π for the Alfvén fire hose; for Alfvén waves we get an estimation based on bi-Maxwellian linear theory $\phi \sim \pi/2$, so we suppose that in the simulation ϕ is a function of time. If we now calculate the correlation between δB and δn for given time t, we get

$$\begin{aligned} \langle \delta B, \delta n\rangle &= \frac{\int_0^{2\pi/k} \delta B \delta n \mathrm{d}x}{\sqrt{\int_0^{2\pi/k}(\delta B)^2\mathrm{d}x \int_0^{2\pi/k}(\delta n)^2\mathrm{d}x}} \\ &= \mathrm{sgn}\big[\cos\phi + \cos(2\omega t+\phi)\big], \end{aligned} \qquad (10)$$

where sgn is the signum function defined as follows:

$$\mathrm{sgn}(x) = \begin{cases} 1 & x > 0 \\ 0 & x = 0 \\ -1 & x < 0. \end{cases} \quad (11)$$

Equation (10) shows that two oppositely propagating waves with $\omega \neq 0$ and ϕ not close to $\pm\pi$ naturally generate a strong oscillation of $\langle \delta B, \delta n \rangle$ between 1 and -1 with the frequency 2ω. In the simulation, there are many modes with different k, ω, ϕ, and amplitudes, and therefore the oscillation of $\langle \delta B, \delta n \rangle$ is smooth and less pronounced. The strongest oscillation appears just at the beginning of the nonlinear phase since the conversion of the strongest Alfvén fire hose modes takes place at similar times and their frequency is similar, close to initial zero frequency; the first oscillation has frequency $2\omega \sim 0.12$.

3.3. Particles

Let us now explore the impact of the wave-particle interaction on the proton distribution function. Plate 6 shows simulated proton distribution functions $v_\perp f(v_\parallel, v_\perp)$ (integrated over all the simulation box), as color scale plot, of the whistler fire hose (left panel) and the Alfvén fire hose (right panel) at the end of the corresponding simulation. First, we look at whistler fire hose. The quasi-linear evolution of whistler fire hose leads to a relatively small change in the proton distribution function (Plate 6, left panel). Figure 1 (left panel) shows there is a small increase in $T_{p\perp}/T_{p\parallel}$. If we look in detail at the proton distribution function (Plate 6, left panel), we find out the distribution function has non-bi-Maxwellian features. The reduced distribution function $f(v_\perp)$ has a power-law-like dependence $\log f \propto -\log v_\perp$ for suprathermal velocities; $f(v_\perp)$ is close to the κ distribution function with the fitted value $\kappa_\perp \sim 150$, which is compatible with a quasi-linear evolution [cf. *Ma and Summers*, 1998]. However, the reduced distribution function $f(v_\parallel)$ is neither Maxwellian nor κ-like; f falls with $v_\parallel$ faster than in the Maxwellian case for suprathermal velocities as a result of cyclotron-resonant, quasi-linear evolution.

The Alfvén fire hose has a more intensive wave-particle interaction than the whistler fire hose (see Figure 1). Therefore it is not surprising that the distribution function presents a strong deviation from a bi-Maxwellian distribution. Indeed, in Plate 6 (right panel) one can easily see protons of $|v_\parallel| \sim 1 - 1.5$ which were accelerated in the perpendicular direction by the Alfvén waves. The reason why the heating is so localized is evident from Plate 4 (bottom panel) and Plate 6: The Alfvén fire hose is generated only for a narrow range of $\boldsymbol{k}$ vectors, and so the resulting Alfvén waves are resonant with protons only in a limited range of (parallel) velocities.

4. Discussion and Conclusion

We have shown that protons with a temperature anisotropy $T_{p\parallel} > T_{p\perp}$ do destabilize not only the well-known whistler fire hose but also the zero-frequency part of the Alfvén branch. The latter instability we call the Alfvén fire hose since it has many properties similar to those of the classical MHD-CGL fire hose. At linear stage the whistler fire hose is generally dominant, but for some plasma parameters the Alfvén fire hose dominates. The Alfvén fire hose shares some similarities with the mirror instability [see, e.g., *Southwood and Kivelson*, 1993] driven by anisotropic protons with $T_{p\parallel} < T_{p\perp}$; in both cases, unstable waves appear for strongly oblique angles with respect to the background magnetic field, they have zero frequency, and the fluctuating magnetic field $\delta\boldsymbol{B}$ and density δn are anticorrelated. The main difference between the two instabilities is that the fluctuating magnetic field $\delta\boldsymbol{B}$ is perpendicular to the background magnetic field $\boldsymbol{B}_0$ for the Alfvén fire hose, whereas for the mirror instability $\delta\boldsymbol{B} \cdot \boldsymbol{B}_0 \neq 0$, and therefore δB^2 and δn are anticorrelated for the mirror instability but not for the Alfvén fire hose.

We have performed 1-D simulations of the whistler fire hose and the Alfvén fire hose. The whistler fire hose saturates in a quasi-linear manner, in agreement with *Quest and Shapiro* [1996] and *Gary et al.* [1998], and then both anisotropy and magnetic fluctuation rest almost constant and no important wave-wave interaction follows. This is probably due to the low amplitude of destabilized waves in our case [cf. *Quest and Shapiro*, 1996]. Such an evolution is largely due to the limitations of 1-D simulations; indeed, *Gary et al.* [1998] have shown that in 2-D there is a slow wave damping and proton heating even after the saturation. *Gary et al.* [1998] interpret these effects as a consequence of the presence of oblique waves which enhance the pitch angle scattering of protons [*Karimabadi et al.*, 1992]. In this article we are mainly concerned with the new instability, the Alfvén fire hose, and for this purpose we perform only 1-D simulations, which allow us to study properties of both instabilities separately.

We have shown that the Alfvén fire hose has a more complicated nonlinear evolution. Alfvén waves have a complicated dispersion including a zero-frequency domain which is destabilized by proton temperature anisotropy. As time goes on and the Alfvén fire hose instability evolves and reaches significant amplitudes, quasi-linear effects heat protons and reduce the anisotropy. This heating changes the dispersion properties of the plasma, and the zero-frequency domain displaces out of the region of instability. The zero-frequency waves are forced to transform themselves to ordinary Alfvén waves, enhancing the proton heating and therefore giving positive feedback to the whole mechanism. The Alfvén waves damp and heat the protons. At later times, Alfvén waves become dispersionless, and a part of the fluctuating energy cascades to longer wavelengths within the Alfvén branch [cf. *Quest and Shapiro*, 1996]. We have seen that the evolution of the Alfvén fire hose can hardly be described as a quasi-linear one, and the final state of the marginal stability is far from the instability threshold, and so the procedure of *Gary et al.* [1998] cannot be simply applied to this instability.

So far we have studied only a plasma with isotropic electrons and anisotropic bi-Maxwellian protons. The influence of electron anisotropy and (anisotropic) minor ions (to say nothing about non-bi-Maxwellian distribution functions) changes the dispersion and growth rates, but we expect the overall nonlinear evolution would be similar (at least for the case of low growth rates, where there is no important particle trapping). Another problem is the competition between the whistler fire hose and the Alfvén fire hose. As the two instabilities have similar growth rates, the nonlinear effects on the competition are important. These problems will be the subject of future work.

Acknowledgments. P.H. thanks the Japan Society for the Promotion of Science and acknowledges grants-in-aid for scientific research 98047 and 08404027.

Janet G. Luhmann thanks Chun-Yu Ma and S. Peter Gary for their assistance in evaluating this paper.

References

Belmont, G., and C. Mazelle, Polytropic indices in collisionless plasmas: Theory and mesuments, *J. Geophys. Res.*, *97*, 8327–8336, 1992.

Gary, S. P., H. Li, S. O'Rourke, and D. Winske, Proton resonant firehose instability: Temperature anisotropy and fluctuating field constraints, *J. Geophys. Res.*, *103*, 14,567–14,574, 1998.

Hellinger, P., and A. Mangeney, Electromagnetic ion beam instabilities: Oblique pulsations, *J. Geophys. Res.*, *104*, 4669–4680, 1999.

Hollweg, J. V., and H. J. Völk, New plasma instabilities in the solar wind, *J. Geophys. Res.*, *75*, 5297–5309, 1970.

Karimabadi, H., D. Krauss-Varban, and T. Teresawa, Physics of pitch angle scattering and velocity diffusion, 1, Theory, *J. Geophys. Res.*, *97*, 13,853–13,864, 1992.

Karimabadi, H., D. Krauss-Varban, and N. Omidi, Characteristic speeds in high beta isotropic/anisotropic plasmas, *Phys. Plasmas*, *2*, 4177–4184, 1995.

Kennel, C. F., and F. L. Scarf, Thermal anisotropies and electromagnetic instabilities in the solar wind, *J. Geophys. Res.*, *73*, 6149, 1968.

Ma, C., and D. Summers, Formation of power-law energy spectra in space plasmas by stochastic acceleration due to whistler-mode waves, *Geophys. Res. Lett.*, *25*, 4099–4102, 1998.

Manheimer, W., and J. P. Boris, Marginal stability analysis: A simpler approach to anomalous transport in plasmas, *Comments Plasma Phys. Controlled Fusion*, *3*, 15–24, 1977.

Matthews, A., Current advance method and cyclic leapfrog for 2D multispecies hybrid plasma simulations, *J. Comput. Phys.*, *112*, 102–116, 1994.

Quest, K. B., and V. D. Shapiro, Evolution of the fire-hose instability: Linear theory and wave-wave coupling, *J. Geophys. Res.*, *101*, 24,457–24,469, 1996.

Rezeau, L., G. Belmont, B. Guéret, and B. Lembège, Cross-bispectral analysis of the electromagnetic field in a beam-plasma interaction, *J. Geophys. Res.*, *102*, 24,387–24,392, 1997.

Southwood, D. J., and M. G. Kivelson, Mirror instability. I – The physical mechanism of linear instability, *J. Geophys. Res.*, *98*, 9181–9187, 1993.

P. Hellinger and H. Matsumoto, Radio Atmospheric Science Center, Kyoto University, Gokanosho, Uji, Kyoto 611-0011, Japan. (helinger@kurasc.kyoto-u.ac.jp; matsumot@kurasc.kyoto-u.ac.jp)